

# PEAfowl: Perception-Enhanced Multi-View Vision-Language-Action for Bimanual Manipulation

Qingyu Fan<sup>1,2</sup>, Zhaoxiang Li<sup>2</sup>, Yi Lu<sup>2</sup>, Wang Chen<sup>2</sup>, Qiu Shen<sup>2</sup>, Xiao-xiao Long<sup>2\*</sup>, Yinghao Cai<sup>1\*</sup>, Tao Lu<sup>1</sup>, Shuo Wang<sup>1</sup> and Xun Cao<sup>2</sup>

<sup>1</sup> Institute of Automation, Chinese Academy of Sciences

<sup>2</sup> Nanjing University

fanqingyu23@mails.ucas.edu.cn, xxlong@nju.edu.cn, yinghao.cai@ia.ac.cn

## Abstract

Bimanual manipulation in cluttered scenes requires policies that remain stable under occlusions, viewpoint and scene variations. Existing vision-language-action models often fail to generalize because (i) multi-view features are fused via view-agnostic token concatenation, yielding weak 3D-consistent spatial understanding, and (ii) language is injected as global conditioning, resulting in coarse instruction grounding. In this paper, we introduce PEAfowl, a perception-enhanced multi-view VLA policy for bimanual manipulation. For spatial reasoning, PEAfowl predicts per-token depth distributions, performs differentiable 3D lifting, and aggregates local cross-view neighbors to form geometrically grounded, cross-view consistent representations. For instruction grounding, we propose to replace global conditioning with a Perceiver-style text-aware readout over frozen CLIP visual features, enabling iterative evidence accumulation. To overcome noisy and incomplete commodity depth without adding inference overhead, we apply training-only depth distillation from a pretrained depth teacher to supervise the depth-distribution head, providing perception front-end with geometry-aware priors. On RoboTwin 2.0 under domain-randomized setting, PEAfowl improves the strongest baseline by 23.0 pp in success rate, and real-robot experiments further demonstrate reliable sim-to-real transfer and consistent improvements from depth distillation. Project website: <https://peafowlvla.github.io/>

## 1 Introduction

Open-world manipulation requires a unified robot policy that integrates vision, language, and proprioception to follow diverse instructions under changing scenes and viewpoints. Recent vision-language-action (VLA) models have shown encouraging performance in single-arm manipulation [Brohan *et al.*, 2023; Zitkovich *et al.*, 2023; Kim *et al.*, 2025;

\*Corresponding authors: Xiao-xiao Long and Yinghao Cai. This work was done while the first author was a visiting student at Nanjing University.

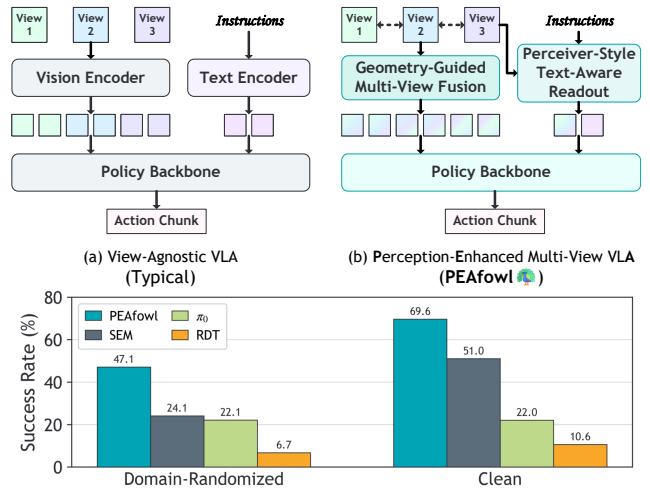
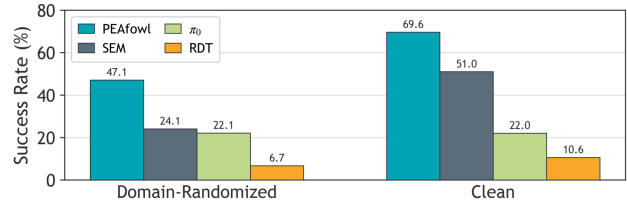


Figure 1: **Motivation and overview of PEAfowl.** (a) Prior bimanual VLAs typically concatenate per-view visual tokens and apply global text conditioning, without explicit cross-view geometric alignment or instruction-relevant visual evidence retrieval and aggregation. (b) We propose PEAfowl, which incorporates geometry-guided multi-view fusion and a Perceiver-style text-as-query readout over frozen CLIP features. Bottom: Average success rates on RoboTwin 2.0 (nine training tasks) under Clean and Domain-Randomized settings, comparing multi-task bimanual baselines.

Ghosh *et al.*, 2024]. By leveraging large-scale robot data and web-scale vision-language supervision, a single policy can now execute a wide range of manipulation skills from natural-language prompts and generalize across simulation and real-world settings.

However, multi-task bimanual manipulation remains underexplored, especially under challenging scene variations. Pretrained VLA policies often exhibit substantial performance degradation in cluttered scenes with distractors and under appearance and viewpoint variations. Generalization to unseen objects or scenes becomes particularly unstable for tasks that require coordinated bimanual motion [Mu *et al.*, 2025; Chen *et al.*, 2025]. The high-dimensional and tightly coupled bimanual action space increases the data requirements for learning generalizable multi-task policies. Moreover, bimanual manipulation often involves frequent self-occlusions and inter-object occlusions as well as fine-



grained language instructions, which place higher demands on perception and vision–language grounding. Under limited demonstrations, improving perception efficiency and grounding fidelity is therefore critical for multi-task and cross-scene generalization.

Bimanual manipulation platforms are inherently multi-view perception systems: multiple cameras are commonly deployed to increase workspace coverage and mitigate occlusions. These complementary views capture rich 3D geometric information that, when properly leveraged, can stabilize spatial understanding across scenes and camera configurations. However, most existing VLA pipelines treat multi-view inputs in a view-agnostic manner: each image is encoded independently, and tokens from different cameras are concatenated or stacked before being passed to a shared policy head [Kim *et al.*, 2025; Lin *et al.*, 2025; Black *et al.*, 2025]. Such designs do not explicitly model cross-view geometric correspondences or enforce 3D consistency in feature space, making the learned representations sensitive to changes in camera poses, calibration errors, and occlusions.

Another key limitation lies in how language interacts with visual features. In many VLA architectures, language is injected as a global conditioning vector or via a small number of text tokens appended to the visual stream, while the dominant attention computation remains vision-centric. This strategy is often sufficient for low-clutter tasks, but in multi-task, multi-object scenes it may produce unfocused, instruction-agnostic attention and weak exploitation of pretrained vision-language alignment to identify relevant objects and spatial relations in the scene. Recent work suggests that text-aware visual feature extraction, in which language tokens explicitly query and aggregate relevant visual evidence, can improve the performance of grounding [Huang *et al.*, 2025], yet such strategies have not been explored for multi-view bimanual manipulation.

In this paper, we introduce PEAfowl, a multi-view vision-language-action model with geometry- and language-guided perception for bimanual manipulation. On the spatial side, we propose a geometry-driven multi-view fusion module that (i) performs per-patch RGB-D token fusion, (ii) predicts a depth distribution for each visual token, and (iii) backprojects tokens into a shared 3D base frame to perform local 3D neighborhood aggregation across cameras. This design explicitly models cross-view geometric correspondences and endows 2D visual features with depth-aware, 3D-consistent structure.

On the language side, PEAfowl builds upon OTTER-style text-aware visual extraction [Huang *et al.*, 2025], and replaces global text conditioning with a Perceiver-style text-aware transformer [Jaegle *et al.*, 2022]. Text tokens act as latent queries that iteratively cross-attend to per-view patch features, producing a compact set of language-conditioned visual tokens. This mechanism sharpens attention over task-relevant objects and spatial relations suitable for policy learning. Fig. 1 provides an overview of this architecture and contrasts it with a standard VLA pipeline.

In real-robot deployment, however, noise and missing measurements from commodity depth sensors can undermine the

benefits of our geometry-aware perception. Our framework naturally supports depth distillation: a stronger depth teacher supervises the predicted per-token depth distributions. We leverage a pretrained Camera Depth Model (CDM) [Liu *et al.*, 2025a] as a training-time depth teacher while still feeding only raw depth images to the policy at both training and test time, which introduces no test-time overhead and transfers refined geometric priors into the multi-view policy.

Both simulation and physical experiments demonstrate that PEAfowl, despite having only **300M** trainable parameters, outperforms existing bimanual VLA models and visuomotor baselines, and generalizes well to novel scene appearances, workspace geometries, and language instructions. In simulation, we evaluate on 9 tasks from RoboTwin 2.0 [Chen *et al.*, 2025] under both clean and heavily domain-randomized settings. On physical platforms, PEAfowl demonstrates consistent sim-to-real transfer, particularly on tasks requiring precise bimanual coordination. To summarize, our contributions are:

1. We introduce a geometry-guided multi-view perception module that builds spatially-aware representations from multi-view RGB-D observations, along with depth distillation scheme for real-world deployment.
2. We propose to replace common global text conditioning in visual-language interaction with a Perceiver-style text-as-query readout over frozen CLIP features, which produces compact instruction-conditioned tokens.
3. Extensive experiments in both simulation and real-world bimanual manipulation tasks demonstrate the benefits of geometry- and language-guided multi-view perception.

## 2 Related Work

### 2.1 Multi-view Perception

Multi-view perception has been studied extensively in classical structure-from-motion and multi-view stereo, and more recently in neural reconstruction and multi-view transformers [Schönberger and Frahm, 2016; Yao *et al.*, 2018; Mildenhall *et al.*, 2020; Wang *et al.*, 2025]. Most of these approaches are typically optimized for offline 3D perception and rely on heavy backbones or dense geometric supervision, which limits their suitability as lightweight perception modules tightly coupled with robot policy learning.

In robotic manipulation, multi-view observations are used to improve robustness to viewpoint variations and mitigate occlusions [Seo *et al.*, 2023; Pang *et al.*, 2025; Qian *et al.*, 2025; Li *et al.*, 2025; Goyal *et al.*, 2023; Goyal *et al.*, 2024; Fan *et al.*, 2025; Lan *et al.*, 2025; Chen *et al.*, 2026]. While these methods demonstrate the benefit of multi-view sensing, many collapse views into view-invariant embeddings or fuse per-view features through simple concatenation, where cross-view 3D consistency is not explicitly considered and depth uncertainty is largely ignored. In contrast, PEAfowl introduces a geometry-guided multi-view perception module that maintains cross-view 3D-aligned spatial tokens under noisy depth measurements.

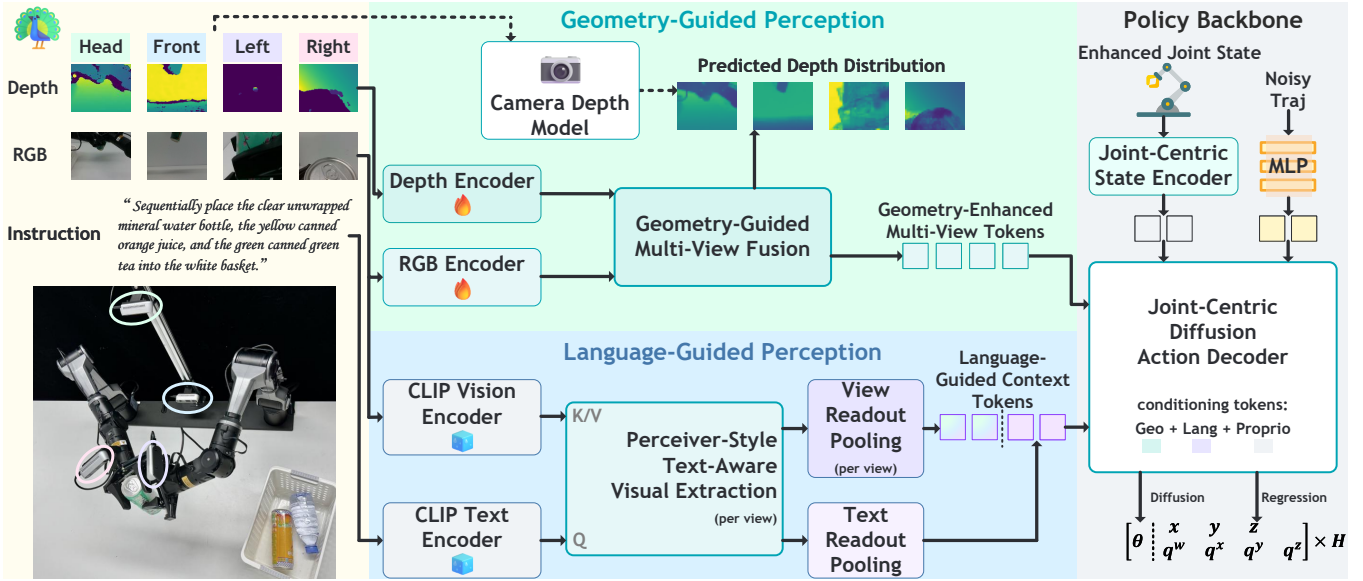


Figure 2: **PEAfowl architecture.** PEAfowl couples geometry-guided multi-view fusion with language-guided readout to condition a SEM-style diffusion action decoder. Top: RGB-D tokens are used to predict per-token depth distributions for differentiable 3D lifting and cross-view fusion; a pretrained camera depth model supervises the depth-distribution head during training only. Bottom: Frozen CLIP features are queried by a Perceiver-style text-as-query readout and pooled into compact context tokens.

## 2.2 Vision-Language-Action Models

VLA policies map visual observations and language instructions to actions [Brohan *et al.*, 2023; Zitkovich *et al.*, 2023; O’Neill *et al.*, 2024]. Existing methods and datasets largely focus on single-arm manipulation. In multi-view settings, images are commonly treated as view-agnostic 2D tokens, with language injected as global conditioning. Recent bi-manual VLAs still rely primarily on 2D RGB features and multi-image concatenation [Liu *et al.*, 2025b; Black *et al.*, 2025]. These approaches often require heavy 3D backbones or strong geometric supervision [Qu *et al.*, 2025; Sun *et al.*, 2025; Yang *et al.*, 2025]. SEM aligns multi-view features and robot states in a shared base frame to form spatial representations [Lin *et al.*, 2025]. For language conditioning, CLIP-RT learns from non-expert language-supervised demonstrations [Kang *et al.*, 2025], and OTTER improves grounding via computing similarity scores between each instruction token and each visual feature to highlight the visual information relevant to the instruction [Huang *et al.*, 2025]. PEAfowl combines 3D-aligned multi-view tokens with iterative text-as-query readout to enable spatial reasoning and more accurate grounding in cluttered bi-manual scenes.

## 3 Methodology

Fig. 2 presents an overview of PEAfowl. The framework integrates geometry-guided multi-view fusion with language-guided readout to produce policy-ready tokens for a joint-centric diffusion action decoder.

### 3.1 Problem Formulation

Let  $\mathcal{V} = \{1, \dots, V\}$  denote the camera set. The robot receives multi-view RGB-D observations  $\mathbf{o}_t \triangleq \{\mathbf{I}_t^{(v)}, \mathbf{D}_t^{(v)}\}_{v \in \mathcal{V}}$ , along with proprioceptive state  $\mathbf{s}_t \in \mathbb{R}^{d_s}$

and instruction  $\ell$ . Our goal is to learn a bi-manual policy  $\pi_\phi$  that predicts an action chunk of horizon  $H$  conditioned on  $(\mathbf{o}_t, \ell, \mathbf{s}_t)$ :

$$\hat{\mathbf{a}}_{t:t+H-1} = \pi_\phi(\mathbf{o}_t, \ell, \mathbf{s}_t). \quad (1)$$

where  $\mathbf{a}_t = [\mathbf{a}_t^L; \mathbf{a}_t^R] \in \mathbb{R}^{d_a}$  concatenates the left- and right-arm control commands.

### 3.2 Geometry-Guided Multi-View Fusion

Bi-manual manipulation in cluttered scenes can be easily affected by self-occlusions and inter-object occlusions, which motivates explicit 3D alignment for multi-view fusion. Given multi-view RGB-D pyramids, our geometry-guided fusion produces spatially consistent tokens via (i) per-patch RGB-D fusion, (ii) per-token depth distributions for differentiable 3D lifting, and (iii) cross-view neighbor aggregation in a shared base frame as shown in Fig. 3.

**Multi-view RGB-D Feature Extraction.** For each view  $v$ , we extract multi-scale RGB and depth feature pyramids with modality-specific encoders shared across cameras. The RGB encoder is initialized from Grounding-DINO [Liu *et al.*, 2024] and depth features are extracted using a lightweight ResNet [He *et al.*, 2016] to obtain  $\{\mathbf{F}_{\text{rgb},l}^{(v)}\}_{l=1}^L$  and  $\{\mathbf{F}_{\text{dep},l}^{(v)}\}_{l=1}^L$ .

**Tokenization across Scales.** We flatten the  $L$ -level feature pyramids into RGB and depth token sequences, denoted by  $\mathbf{T}_{\text{rgb}}^{(v)} = \{\mathbf{t}_{\text{rgb},n}^{(v)}\}$  and  $\mathbf{T}_{\text{dep}}^{(v)} = \{\mathbf{t}_{\text{dep},n}^{(v)}\}$ . Known camera intrinsics and extrinsics are used for backprojection in the subsequent 3D lifting.

**Depth-Aware 3D Lifting.** To model depth ambiguity at the patch level, we predict a discrete depth distribution  $\mathbf{p}_n^{(v)}$  over  $B$  bins from co-located RGB-D token pairs, and use it to

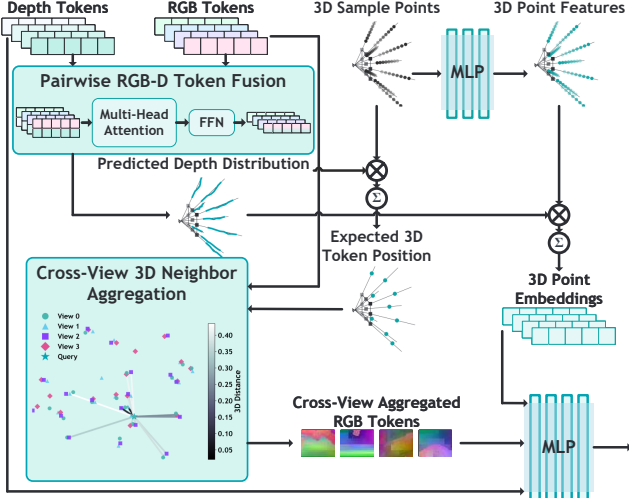


Figure 3: **Geometry-Guided Multi-View Fusion (GGMVF).** Multi-scale RGB and depth features are tokenized, and co-located RGB-D pairs are used to predict discrete depth distributions for differentiable 3D lifting. The resulting 3D anchors enable top- $K$  cross-view neighbor aggregation in the base frame using distance-based softmax weights and a gated residual update. Aggregated RGB tokens are fused with depth tokens and 3D point embeddings via an MLP to produce geometry-enhanced tokens.

softly lift each 2D token into the robot base frame. For view  $v$  and token  $n$ , the token center  $\mathbf{u}_n^{(v)}$  is backprojected at each depth bin  $d_i$  to obtain 3D samples  $\mathbf{x}_{n,i}^{(v)}$ . We then compute the expected 3D anchor and a depth-aware point embedding by distribution-weighted aggregation:

$$\bar{\mathbf{x}}_n^{(v)} = \sum_{i=1}^B p_{n,i}^{(v)} \mathbf{x}_{n,i}^{(v)}, \quad \mathbf{g}_n^{(v)} = \sum_{i=1}^B p_{n,i}^{(v)} \phi(\mathbf{x}_{n,i}^{(v)}). \quad (2)$$

where  $\phi(\cdot)$  projects 3D coordinates to point features. We use  $\bar{\mathbf{x}}_n^{(v)}$  for cross-view matching and  $\mathbf{g}_n^{(v)}$  as geometric context for subsequent fusion.

**Pairwise RGB-D Token Fusion.** To incorporate noisy commodity depth measurements without corrupting pre-trained RGB semantics, we apply a lightweight *local* fusion only on co-located RGB-D token pairs and only in the depth-distribution branch. The RGB token is projected to the depth feature dimension and fused with the length-2 pair using a small attention block:

$$[\hat{\mathbf{r}}_n^{(v)}, \hat{\mathbf{d}}_n^{(v)}] = \text{PairAttn}([\mathbf{W}_r \mathbf{t}_{\text{rgb},n}^{(v)}, \mathbf{t}_{\text{dep},n}^{(v)}]). \quad (3)$$

By restricting attention to co-located RGB-D pairs, the fusion learns reliable mixing while leaving the main RGB stream unchanged.

**Cross-View 3D Neighbor Aggregation.** Given expected 3D token anchors  $\{\bar{\mathbf{x}}_n^{(v)}\}$  from Eq. (2), we aggregate information across views based on geometric proximity in the shared base frame. For each query token  $(v, n)$ , we compute pairwise distances  $\delta_{n,m}^{(v,w)} = \|\bar{\mathbf{x}}_n^{(v)} - \bar{\mathbf{x}}_m^{(w)}\|_2$  to tokens  $(w, m)$  from other views, select the  $K$  nearest neighbors  $\mathcal{N}_n^{(v)}$ , and

aggregate their RGB tokens with a distance-softmax:

$$\alpha_{n,m}^{(v,w)} = \frac{\exp(-\delta_{n,m}^{(v,w)}/\tau)}{\sum_{(w',m') \in \mathcal{N}_n^{(v)}} \exp(-\delta_{n,m'}^{(v,w')}/\tau)}. \quad (4)$$

where  $\tau$  controls the softness of geometric matching. The aggregated feature is then computed as:

$$\mathbf{h}_n^{(v)} = \sum_{(w,m) \in \mathcal{N}_n^{(v)}} \alpha_{n,m}^{(v,w)} \mathbf{t}_{\text{rgb},m}^{(w)}. \quad (5)$$

The aggregated feature is then added to the original token via a gated residual update:

$$\tilde{\mathbf{t}}_{\text{rgb},n}^{(v)} = \mathbf{t}_{\text{rgb},n}^{(v)} + \gamma \mathbf{h}_n^{(v)}. \quad (6)$$

where  $\gamma$  is a learnable scalar gate. This geometry-based aggregation aligns tokens that correspond to the same physical region across cameras, thereby improving robustness to occlusions and viewpoint changes. The resulting tokens are fused with depth tokens and 3D point embeddings via an MLP to form inputs to the action decoder.

### 3.3 Language-Guided Multi-View Readout

To improve instruction grounding in cluttered multi-object scenes, we replace global text conditioning with a text-aware multi-view readout over frozen CLIP features. For each view, we use a Perceiver-style extractor that iteratively updates text latents by cross-attending to CLIP patch tokens, yielding compact instruction-conditioned tokens for the policy.

**Frozen CLIP Tokens.** Given instruction  $\ell$  and multi-view RGB images  $\{\mathbf{I}^{(v)}\}_{v \in \mathcal{V}}$ , we extract frozen CLIP text tokens and per-view patch tokens. For denser vision-language alignment, we use the final attention-layer outputs of the CLIP vision encoder [Lan *et al.*, 2024]:

$$\mathbf{T}_{\text{txt}} = \text{CLIP}_{\text{txt}}(\ell) \in \mathbb{R}^{K_{\text{txt}} \times D_c}, \quad (7)$$

$$\mathbf{X}^{(v)} = \text{CLIP}_{\text{img}}^{\text{attn-last}}(\mathbf{I}^{(v)}) \in \mathbb{R}^{N_p \times D_c}. \quad (8)$$

**Perceiver-Style Text-as-Query Readout.** For each view  $v$ , latent queries are initialized with text tokens and refined through  $M$  latent blocks that alternate cross-attention to patches and latent self-attention:

$$\mathbf{Z}^{(v,0)} = \mathbf{T}_{\text{txt}}, \quad (9)$$

$$\mathbf{Z}^{(v,m+1)} = \text{LatentBlock}(\mathbf{Z}^{(v,m)}, \mathbf{X}^{(v)}), \quad m = 0, \dots, M-1, \quad (10)$$

which produce vision-grounded text latents  $\mathbf{Z}^{(v)} \triangleq \mathbf{Z}^{(v,M)} \in \mathbb{R}^{K_{\text{txt}} \times D_c}$ . ReZero-gated residuals are used for stable stacking [Bachlechner *et al.*, 2021].

**Readout Tokens.** We summarize tokens into a fixed number of context tokens via attention pooling:

$$\mathbf{R}^{(v)} = \text{Pool}(\mathbf{Z}^{(v)}) \in \mathbb{R}^{R \times d}, \quad \mathbf{R}_{\text{txt}} = \text{Pool}(\mathbf{T}_{\text{txt}}) \in \mathbb{R}^{R \times d}. \quad (11)$$

and concatenate them as the language-guided context sequence:

$$\mathbf{S} = [\mathbf{R}_{\text{txt}}; \mathbf{R}^{(1)}; \dots; \mathbf{R}^{(V)}] \in \mathbb{R}^{(R+V \times R) \times d}. \quad (12)$$

which conditions the action decoder together with geometry-enhanced tokens (Sec. 3.2) and proprioception.

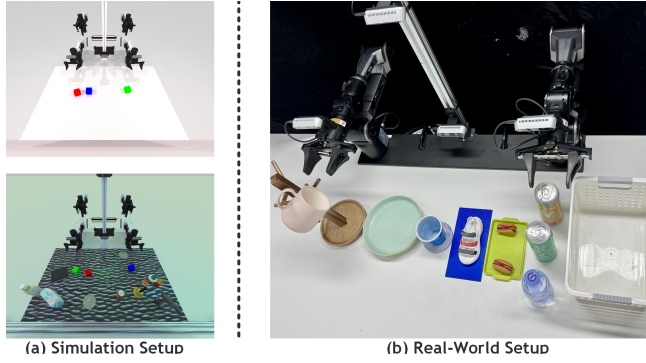


Figure 4: **Simulation and real-world setups.** (a) RoboTwin 2.0 simulation (Aloha-AgileX, 4-camera RGB-D) under Clean (top) and Domain-Randomized (bottom) settings. (b) Dual-arm AgileX Piper with a 4-camera rig.

### 3.4 Policy Backbone

The policy backbone follows SEM’s joint-centric state encoder and diffusion action decoder [Lin *et al.*, 2025].

**Joint-Centric State.** The robot state at time  $t$  is represented as  $\mathbf{J}_t = [\mathbf{J}_{t,i}]_{i=1}^{N_j} \in \mathbb{R}^{N_j \times 8}$ , where each joint token is defined as:

$$\mathbf{J}_{t,i} = [\theta_{t,i}; \mathbf{p}_{t,i}; \mathbf{q}_{t,i}], \quad \mathbf{p}_{t,i} \in \mathbb{R}^3, \quad \mathbf{q}_{t,i} \in \mathbb{R}^4. \quad (13)$$

Here  $(\mathbf{p}_{t,i}, \mathbf{q}_{t,i})$  is the joint-frame pose in the robot base frame obtained via forward kinematics.

**State Encoder and Action Decoder.** An MLP and joint-graph attention (with link-hop distances  $\mathbf{G} \in \mathbb{R}^{N_j \times N_j}$ ) encode  $\mathbf{J}_t$  into state tokens  $\mathbf{E}_t \in \mathbb{R}^{N_j \times d}$ . A joint-centric diffusion transformer predicts an  $H$ -step trajectory, using self- and temporal attention, and cross-attention to geometry-enhanced multi-view tokens (Sec. 3.2) and language-guided context tokens (Sec. 3.3); during training we diffuse joint angles and recompute noisy poses via forward kinematics.

### 3.5 Training Objectives

We optimize PEAfowl with a joint-centric diffusion imitation objective for policy learning and an auxiliary depth distillation loss for geometry-guided perception.

**Diffusion Imitation Loss.** The diffusion decoder predicts an  $H$ -step bimanual joint trajectory. Given a noisy input, the decoder outputs the denoised sequence  $\hat{\mathbf{J}}_{t:t+H-1}$ . Training minimizes a weighted regression loss:

$$\mathcal{L}_{\text{diff}} = \left\| (\hat{\mathbf{J}} - \mathbf{J}) \mathbf{W} \right\|_2^2. \quad (14)$$

where  $\mathbf{W}$  is a diagonal weight matrix. Optionally, we add a forward-kinematics consistency term by recomputing joint poses from the predicted joint angles:

$$\mathcal{L}_{\text{fk}} = \left\| (\text{FK}(\hat{\theta}_{t:t+H-1}) - \mathbf{J}_{t:t+H-1}^{\text{pose}}) \mathbf{W}_{\text{fk}} \right\|_2^2. \quad (15)$$

**Depth Distillation with Camera Depth Models.** Our geometry-guided branch predicts a per-token depth distribution  $\mathbf{p}_n^{(v)}$  (Sec. 3.2), which is well suited for depth distillation from a pretrained depth teacher to inject geometry-aware

Table 1: **Simulation results on RoboTwin 2.0.** Success rate (%) under Clean and DR (domain-randomized) settings. Task abbreviations: OM=Open Microwave, SB3=Stack Blocks Three, SW3=Stack Bowls Three, BR-RGB=Blocks Ranking RGB, BR-Size=Blocks Ranking Size, HM=Hanging Mug, OL=Open Laptop, PBF=Place Burger Fries, PEC=Place Empty Cup.

Horizon	Task	DP	DP3	ACT	$\pi_0$	RDT	SEM	PEAfowl
		Clean						
Long	OM	5	61	<b>86</b>	25	9	17	<b>70</b>
	SB3	0	1	0	2	0	<b>29</b>	<b>72</b>
	SW3	63	57	48	47	19	<b>68</b>	<b>79</b>
	BR-RGB	0	3	1	16	0	<b>55</b>	<b>84</b>
	BR-Size	1	2	0	4	0	<b>21</b>	<b>27</b>
	Long Avg.	13.8	24.8	27.0	18.8	5.6	<b>38.0</b>	<b>66.4</b>
Mid	HM	8	17	7	6	0	<b>24</b>	<b>41</b>
	OL	49	<b>82</b>	56	38	25	<b>75</b>	<b>77</b>
	Mid Avg.	28.5	<b>49.5</b>	31.5	22.0	12.5	<b>49.5</b>	<b>59.0</b>
Short	PBF	72	72	49	28	19	<b>93</b>	<b>95</b>
	PEC	37	65	61	32	23	<b>77</b>	<b>81</b>
	Short Avg.	54.5	68.5	55.0	30.0	21.0	<b>85.0</b>	<b>88.0</b>
	Avg.	26.1	40.0	34.2	22.0	10.6	<b>51.0</b>	<b>69.6</b>
DR								
Long	OM	0	22	17	8	8	<b>25</b>	<b>34</b>
	SB3	0	0	0	<b>15</b>	0	1	<b>34</b>
	SW3	30	8	8	<b>48</b>	6	41	<b>66</b>
	BR-RGB	0	0	0	4	0	<b>15</b>	<b>47</b>
	BR-Size	0	1	0	<b>10</b>	0	0	<b>14</b>
	Long Avg.	6.0	6.2	5.0	<b>17.0</b>	2.8	16.4	<b>39.0</b>
Mid	HM	1	9	2	6	3	<b>18</b>	<b>26</b>
	OL	32	<b>61</b>	18	45	31	<b>61</b>	<b>68</b>
	Mid Avg.	16.5	35.0	10.0	25.5	17.0	<b>39.5</b>	<b>47.0</b>
Short	PBF	38	21	22	31	9	<b>46</b>	<b>65</b>
	PEC	1	5	3	<b>32</b>	3	10	<b>70</b>
	Short Avg.	19.5	13.0	12.5	<b>31.5</b>	6.0	28.0	<b>67.5</b>
	Avg.	11.3	14.1	7.8	22.1	6.7	<b>24.1</b>	<b>47.1</b>

priors into the policy. We adopt the Camera Depth Model (CDM) from [Liu *et al.*, 2025a] and preprocess the training set offline to obtain refined depths  $\tilde{\mathbf{D}}^{(v)} = f_{\text{CDM}}(\mathbf{I}^{(v)}, \mathbf{D}^{(v)})$ , from which we derive soft depth-bin targets  $\mathbf{q}_n^{(v)}$ . During both training and inference, the policy input remains the raw depth  $\mathbf{D}^{(v)}$ , incurring no inference overhead. The depth distribution is supervised with a validity-weighted soft-label BCE loss:

$$\mathcal{L}_{\text{depth}} = \frac{1}{VN} \sum_{v \in \mathcal{V}} \sum_{n=1}^N \omega_n^{(v)} \cdot \text{BCE}(\mathbf{p}_n^{(v)}, \mathbf{q}_n^{(v)}). \quad (16)$$

**Total Loss.** The overall training objective combines diffusion imitation, FK consistency, and depth distillation:

$$\mathcal{L} = \mathcal{L}_{\text{diff}} + \lambda_{\text{fk}} \mathcal{L}_{\text{fk}} + \lambda_{\text{depth}} \mathcal{L}_{\text{depth}}. \quad (17)$$

## 4 Experiments

### 4.1 Experimental Setup

**Simulation Setup.** We evaluate our method in simulation on RoboTwin 2.0 [Chen *et al.*, 2025], a scalable benchmark for bimanual manipulation. Two environment settings are used: Clean and Domain-Randomized (DR). The clean setting uses fixed visual and physical parameters with templated

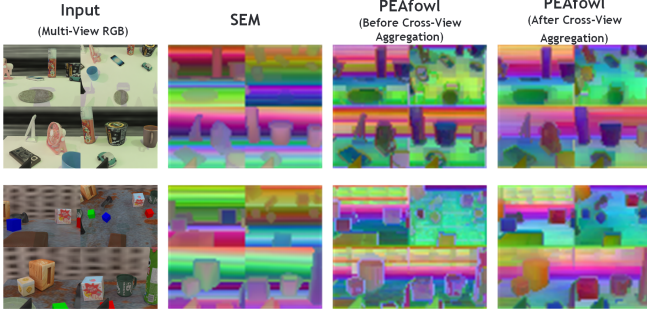


Figure 5: **Cross-view token consistency.** Compared with SEM and PEAfowl pre-aggregation, PEAfowl post-aggregation yields more view-consistent, 3D-aligned clusters for the same physical regions across cameras.

Table 2: **Generalization to held-out tasks.** Success rates (%) on two unseen tasks under Clean and DR, trained on the nine-task suite. Task abbr: SB2=Stack Blocks Two, SW2=Stack Bowls Two.

Task	Setting	$\pi_0$	RDT	SEM	PEAfowl
SB2	Clean	25	0	49	74
	DR	34	0	14	51
SW2	Clean	83	38	93	97
	DR	79	23	65	82

instructions for in-distribution evaluation, while the DR setting applies strong structured perturbations, e.g., distractors, lighting, texture, tabletop height, and instruction paraphrases, to stress-test robustness and cross-scene generalization. All simulation experiments use the Aloha-AgileX embodiment with a 4-camera RGB-D setup. Unless otherwise specified, results are reported on 9 tasks spanning short-, mid-, and long-horizon interactions, with 50 demonstrations per task. VLA models are trained jointly across all tasks, while visuomotor policies are trained separately for each task.

**Real-World Setup.** Experiments are conducted on a dual-arm AgileX Piper platform that mirrors the simulation configuration. Our real-robot setting includes 6 tasks: 4 adapted from simulation for sim-to-real evaluation, and 2 real-only tasks included in the real-world training data. We collect 100 high-quality demonstrations per task via VR teleoperation. Methods are initialized from simulation-pretrained models and then fine-tuned separately for each task on the corresponding real-world dataset. To verify effectiveness when multi-view overlap is reduced, we narrow each camera’s field of view, increasing the difficulty of the real-robot experiments. Fig. 4 provides an overview of the real-world setup.

**Baselines.** We compare PEAfowl with visuomotor and bimanual VLA baselines. Visuomotor policies include ACT [Zhao *et al.*, 2023], DP [Chi *et al.*, 2023], and DP3 [Ze *et al.*, 2024], trained separately per task. VLA baselines trained jointly across tasks include  $\pi_0$  [Black *et al.*, 2025], RDT [Liu *et al.*, 2025b], and SEM [Lin *et al.*, 2025]. All baselines use the same observation setup, training splits, and sim-to-real fine-tuning protocol as PEAfowl.

**Metrics.** In simulation, we run 100 trials per task per setting, and on real-robot experiments 10 trials per task. We

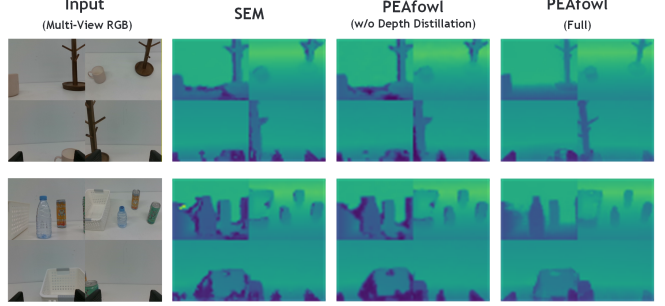


Figure 6: **Depth-distribution predictions (real robot).** Predicted per-token depth distributions for SEM, PEAfowl w/o depth distillation, and full PEAfowl. PEAfowl produces cleaner predictions than SEM, and training-only depth distillation further sharpens and completes depth under noisy commodity sensors.

Table 3: **Real-world results.** Success rates (%) on the dual-arm platform. Task abbr.: PS=Place Shoe, PBD=Put Bottles Dustbin.

Task	PEAfowl	PEAfowl w/o DD	SEM
SW3	<b>100 (10/10)</b>	<u>70 (7/10)</u>	30 (3/10)
HM	<b>30 (3/10)</b>	<u>10 (1/10)</u>	0 (0/10)
PBF	<b>60 (6/10)</b>	<u>30 (3/10)</u>	10 (1/10)
PEC	<b>80 (8/10)</b>	<u>50 (5/10)</u>	20 (2/10)
PS	<b>60 (6/10)</b>	<u>30 (3/10)</u>	10 (1/10)
PBD	<b>80 (8/10)</b>	<u>30 (3/10)</u>	0 (0/10)
Avg.	<b>68.3</b>	<u>36.7</u>	11.7

report **Success Rate**, the fraction of trials that finish the task within the episode time limit. Full implementation details are provided in the Appendix.

## 4.2 Results and Analysis

**Simulation Results.** As shown in Tab. 1, under the RoboTwin 2.0 DR setting, PEAfowl achieves an average success rate of **47.1%** across 9 tasks, consistently outperforming all baselines. In contrast, task-specific visuomotor policies trained per task rarely succeed on these challenging tasks, which indicates that limited demonstrations are insufficient to handle appearance and layout variations.

Among multi-task bimanual VLA baselines,  $\pi_0$  achieves an average of 22.1% under the DR setting, indicating that large-scale vision-language and robot-data pretraining improve cross-scene generalization, whereas RDT underperforms under heavy randomization. SEM is the strongest baseline, which leverages 3D spatial position embeddings along with a joint-centric state encoder and action decoder.

PEAfowl improves over SEM by **23.0 pp**, with particularly large gains on long-horizon and occlusion-heavy tasks. Notably, on visually similar yet instruction-distinct tasks (**Stack Blocks Three** vs. **Blocks Ranking RGB**),  $\pi_0$  and SEM exhibit task-specific biases, whereas PEAfowl performs well on both, suggesting more reliable instruction grounding and robustness to clutter and occlusions.

We further visualize multi-view token embeddings before and after cross-view aggregation using t-SNE as shown in Fig. 5. After aggregation, tokens corresponding to the same physical regions across views cluster more coherently, indicating that geometry-guided fusion yields more view-

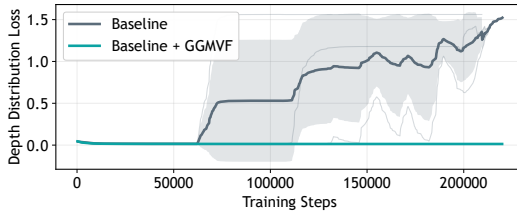


Figure 7: Depth-loss stability. Under multi-task training, the Baseline’s depth loss diverges, while adding GGMVF stabilizes depth-distribution learning.

consistent, 3D-aligned representations under distractors and viewpoint changes.

In the clean setting, where the goal is to evaluate in-distribution task competence, PEAfowl achieves **69.6%** average success, surpassing SEM by **18.6 pp**. The improvements are most obvious on long-horizon tasks which demand maintaining consistent spatial awareness under repeated occlusions and viewpoint changes, while gains on short-horizon tasks are smaller due to an already high baseline performance. Consistent with the DR evaluation, PEAfowl better identifies instruction-relevant targets and relations in referentially ambiguous scenes, showing less dependence on task priors.

Finally, we evaluate in-domain task generalization on two additional tasks not included in the nine-task training set in Tab. 2. PEAfowl consistently outperforms all baselines under both clean and DR settings. Notably, for **Stack Blocks Two** under DR, SEM drops from 49% to 14%, while PEAfowl maintains 51%, indicating better transfer of spatial and semantic information to unseen but related bimanual tasks.

**Real-World Results.** Tab. 3 compares PEAfowl with SEM, the strongest baseline in simulation, and further ablates training-only depth distillation (DD). PEAfowl outperforms SEM on all 6 real-robot tasks, indicating more reliable sim-to-real transfer with real-world commodity depth sensors. DD brings additional improvements, particularly on depth-sensitive tasks such as **Put Bottles Dustbin** and **Hanging Mug**. Fig. 6 visualizes an example of depth-distribution prediction, suggesting that distillation injects geometric priors from a pretrained depth teacher and improves spatial perception without adding test-time overhead.

We also observe that SEM suffers depth-loss divergence during real-robot fine-tuning (cf. Section 4.3), highlighting the difficulty of learning stable depth-aware representations from noisy sensor depth alone. In contrast, PEAfowl’s local RGB-D pairwise fusion and cross-view 3D neighbor aggregation mitigate unreliable depth and stabilize multi-view spatial reasoning. Qualitative rollouts are provided in the supplementary video.

### 4.3 Ablation Studies

We ablate PEAfowl on RoboTwin 2.0 by removing individual components from the full model and by adding our geometry-guided perception to a simple visuomotor baseline. The baseline excludes both the language branch and the geometry-guided pathway (pairwise RGB-D fusion and cross-view 3D neighbor aggregation). We evaluate three variants: (i) replacing the Perceiver-style iterative readout with OTTER’s

Table 4: **Ablations on RoboTwin 2.0.** Success rate (%) on nine tasks under Clean and DR. Task abbreviations follow Table 1.

Task	PEAfowl	w/ 1-step		Baseline	
		SimAttn	w/o VG-Text	+ GGMVF	Baseline
<b>Clean</b>					
OM	<b>70</b>	44	<u>65</u>	45	17
SB3	<b>72</b>	<u>70</u>	39	21	1
SW3	<b>79</b>	71	75	<u>77</u>	50
BR-RGB	<b>84</b>	<u>75</u>	62	69	44
BR-Size	<b>27</b>	<u>26</u>	<b>27</b>	21	16
HM	<b>41</b>	38	<u>40</u>	39	29
OL	<b>77</b>	74	<u>76</u>	<u>76</u>	<u>76</u>
PBF	<b>95</b>	<b>98</b>	<b>98</b>	94	<u>95</u>
PEC	<b>81</b>	<u>79</u>	<u>79</u>	77	74
<b>Avg.</b>	<b>69.6</b>	<u>63.9</u>	62.3	57.7	44.7
<b>DR</b>					
OM	<b>34</b>	31	<u>32</u>	26	17
SB3	<b>34</b>	18	<u>26</u>	7	1
SW3	<b>66</b>	<u>61</u>	<u>61</u>	<u>61</u>	50
BR-RGB	<b>47</b>	<u>35</u>	31	34	11
BR-Size	<b>14</b>	1	3	<u>7</u>	0
HM	<b>26</b>	19	20	<u>23</u>	14
OL	<b>68</b>	<u>65</u>	<b>68</b>	<b>68</b>	<b>68</b>
PBF	<b>65</b>	<u>49</u>	<u>49</u>	44	<b>65</b>
PEC	<b>70</b>	46	<u>60</u>	52	56
<b>Avg.</b>	<b>47.1</b>	36.1	<u>38.9</u>	35.8	31.3

one-step similarity readout (**w/ 1-step SimAttn**); (ii) removing vision-grounded text tokens and conditioning the policy only on instruction-summary tokens (**w/o VG-Text**); and (iii) adding the full geometry-guided module to the baseline (**Baseline+GGMVF**).

As shown in Tab. 4, **w/ 1-step SimAttn** yields a small degradation under the clean setting but a substantially larger drop under DR, highlighting the need for iterative, text-aware evidence accumulation under clutter and scene shifts. **w/o VG-Text** also lowers success, with more obvious drop on attribute- and reference-sensitive tasks, demonstrating the importance of text-aware visual extraction. Finally, while the baseline suffers from depth-loss divergence and collapsed depth distributions (Fig. 7), **Baseline+GGMVF** remains stable and improves long-horizon performance, indicating that our geometry-guided pathway is important for reliable depth-aware multi-task learning. We further ablate camera views under the DR setting: removing the front view consistently hurts success, and removing both wrist views leads to a larger drop. Detailed averages and per-task results are reported in the Appendix.

## 5 Conclusions

In this paper, we proposed PEAfowl, a perception-enhanced multi-view VLA policy for bimanual manipulation that generalizes under clutter, occlusions, and scene variations. PEAfowl couples geometry-guided fusion to maintain a consistent cross-view 3D spatial belief with a Perceiver-style text-as-query readout on frozen CLIP features for improved instruction grounding. Across RoboTwin 2.0 and real-robot evaluations, PEAfowl achieves state-of-the-art success rates and reliable sim-to-real transfer, with ablations highlighting the contributions of both components and multi-view sensing.

## References

[Bachlechner *et al.*, 2021] Thomas Bachlechner, Bodhisattwa Prasad Majumder, Henry Mao, Gary Cottrell, and Julian McAuley. ReZero is all you need: Fast convergence at large depth. In *Proceedings of the 37th Conference on Uncertainty in Artificial Intelligence (UAI)*, volume 161 of *Proceedings of Machine Learning Research*. PMLR, 2021.

[Black *et al.*, 2025] Kevin Black, Noah Brown, Danny Driess, Adnan Esmail, Michael Robert Equi, Chelsea Finn, Niccolò Fusai, Lachy Groom, Karol Hausman, Brian Ichter, et al.  $\pi_0$ : A Vision-Language-Action Flow Model for General Robot Control. In *Proceedings of Robotics: Science and Systems*, LosAngeles, CA, USA, June 2025.

[Brohan *et al.*, 2023] Anthony Brohan, Noah Brown, Justice Carbal, Yevgen Chebotar, Joseph Dabis, Chelsea Finn, Keerthana Gopalakrishnan, Karol Hausman, Alexander Herzog, Jasmine Hsu, et al. RT-1: Robotics Transformer for Real-World Control at Scale. In *Proceedings of Robotics: Science and Systems*, Daegu, Republic of Korea, July 2023.

[Chen *et al.*, 2025] Tianxing Chen, Zanxin Chen, Baijun Chen, Zijian Cai, Yibin Liu, Zixuan Li, Qiwei Liang, Xianliang Lin, Yiheng Ge, Zhenyu Gu, et al. Robotwin 2.0: A scalable data generator and benchmark with strong domain randomization for robust bimanual robotic manipulation. *arXiv preprint arXiv:2506.18088*, 2025.

[Chen *et al.*, 2026] Haoyuan Chen, Rushuai Yang, Junjie Zhang, Xiaoyu Wen, Yi Chen, Dengxiu Yu, Chenjia Bai, and Zhen Wang. Temporal consistent multi-view perception for robust embodied manipulation. *Pattern Recognition*, 171:112177, 2026.

[Chi *et al.*, 2023] Cheng Chi, Siyuan Feng, Yilun Du, Zhenjia Xu, Eric Cousineau, Benjamin CM Burchfiel, and Shuran Song. Diffusion Policy: Visuomotor Policy Learning via Action Diffusion. In *Proceedings of Robotics: Science and Systems*, Daegu, Republic of Korea, July 2023.

[Fan *et al.*, 2025] Qingyu Fan, Yinghao Cai, Chao Li, Wenzhe He, Xudong Zheng, Tao Lu, Bin Liang, and Shuo Wang. Neugrasp: Generalizable neural surface reconstruction with background priors for material-agnostic object grasp detection. In *2025 IEEE International Conference on Robotics and Automation (ICRA)*, pages 3197–3203, 2025.

[Ghosh *et al.*, 2024] Dibya Ghosh, Homer Rich Walke, Karl Pertsch, Kevin Black, Oier Mees, Sudeep Dasari, Joey Hejna, Tobias Kreiman, Charles Xu, Jianlan Luo, You Liang Tan, Lawrence Yunliang Chen, Quan Vuong, Ted Xiao, Pannag R Sanketi, Dorsa Sadigh, Chelsea Finn, and Sergey Levine. Octo: An Open-Source Generalist Robot Policy. In *Proceedings of Robotics: Science and Systems*, Delft, Netherlands, July 2024.

[Goyal *et al.*, 2023] Ankit Goyal, Jie Xu, Yijie Guo, Valts Blukis, Yu-Wei Chao, and Dieter Fox. RVT: Robotic view transformer for 3D object manipulation. In *Proceedings of The 7th Conference on Robot Learning*, volume 229 of *Proceedings of Machine Learning Research*, pages 694–710. PMLR, 2023.

[Goyal *et al.*, 2024] Ankit Goyal, Valts Blukis, Jie Xu, Yijie Guo, Yu-Wei Chao, and Dieter Fox. RVT-2: Learning Precise Manipulation from Few Demonstrations. In *Proceedings of Robotics: Science and Systems*, Delft, Netherlands, July 2024.

[He *et al.*, 2016] Kaiming He, Xiangyu Zhang, Shaoqing Ren, and Jian Sun. Deep residual learning for image recognition. In *Proceedings of the IEEE Conference on Computer Vision and Pattern Recognition (CVPR)*, pages 770–778, 2016.

[Huang *et al.*, 2025] Huang Huang, Fangchen Liu, Letian Fu, Tingfan Wu, Mustafa Mukadam, Jitendra Malik, Ken Goldberg, and Pieter Abbeel. OTTER: A vision-language-action model with text-aware visual feature extraction. In *Proceedings of the 42nd International Conference on Machine Learning*, volume 267 of *Proceedings of Machine Learning Research*. PMLR, 2025.

[Jaegle *et al.*, 2022] Andrew Jaegle, Sebastian Borgeaud, Jean-Baptiste Alayrac, Carl Doersch, Catalin Ionescu, David Ding, Skanda Koppula, Daniel Zoran, Andrew Brock, Evan Shelhamer, Olivier J. Henaff, Matthew Botvinick, Andrew Zisserman, Oriol Vinyals, and Joao Carreira. Perceiver IO: A general architecture for structured inputs & outputs. In *International Conference on Learning Representations*, 2022.

[Kang *et al.*, 2025] Gi-Cheon Kang, Junghyun Kim, Kyuhwan Shim, Jun Ki Lee, and Byoung-Tak Zhang. CLIP-RT: Learning Language-Conditioned Robotic Policies from Natural Language Supervision. In *Proceedings of Robotics: Science and Systems*, LosAngeles, CA, USA, June 2025.

[Kim *et al.*, 2025] Moo Jin Kim, Karl Pertsch, Siddharth Karamcheti, Ted Xiao, Ashwin Balakrishna, Suraj Nair, Rafael Rafailov, Ethan Foster, Grace Lam, Pannag Sanketi, et al. OpenVLA: An open-source vision-language-action model. In *Proceedings of The 8th Conference on Robot Learning*, volume 270 of *Proceedings of Machine Learning Research*, pages 2679–2713. PMLR, 2025.

[Lan *et al.*, 2024] Mengcheng Lan, Chaofeng Chen, Yiping Ke, Xinjiang Wang, Litong Feng, and Wayne Zhang. ClearCLIP: Decomposing CLIP representations for dense vision-language inference. In *Proceedings of the European Conference on Computer Vision (ECCV)*, 2024.

[Lan *et al.*, 2025] Zihan Lan, Weixin Mao, Haosheng Li, Le Wang, Tiancai Wang, Haoqiang Fan, and Osamu Yoshie. Bfa: Best-feature-aware fusion for multi-view fine-grained manipulation. *arXiv preprint arXiv:2502.11161*, 2025.

[Li *et al.*, 2025] Zheng Li, Pei Qu, Yufei Jia, Shihui Zhou, Haizhou Ge, Jiahang Cao, Jinni Zhou, Guyue Zhou, and Jun Ma. Manivid-3d: Generalizable view-invariant reinforcement learning for robotic manipulation via disentangled 3d representations. *arXiv preprint arXiv:2509.11125*, 2025.

[Lin *et al.*, 2025] Xuewu Lin, Tianwei Lin, Lichao Huang, Hongyu Xie, Yiwei Jin, Keyu Li, and Zhizhong Su. SEM: Enhancing spatial understanding for robust robot manipulation. *arXiv preprint arXiv:2505.16196*, 2025.

[Liu *et al.*, 2024] Shilong Liu, Zhaoyang Zeng, Tianhe Ren, Feng Li, Hao Zhang, Jie Yang, Qing Jiang, Chunyuan Li, Jianwei Yang, Hang Su, et al. Grounding DINO: Marrying DINO with grounded pre-training for open-set object detection. In *Proceedings of the European Conference on Computer Vision (ECCV)*, 2024.

[Liu *et al.*, 2025a] Minghuan Liu, Zhengbang Zhu, Xiaoshen Han, Peng Hu, Haotong Lin, Xinyao Li, Jingxiao Chen, Jiafeng Xu, Yichu Yang, Yunfeng Lin, et al. Manipulation as in simulation: Enabling accurate geometry perception in robots. *arXiv preprint arXiv:2509.02530*, 2025.

[Liu *et al.*, 2025b] Songming Liu, Lingxuan Wu, Bangguo Li, Hengkai Tan, Huayu Chen, Zhengyi Wang, Ke Xu, Hang Su, and Jun Zhu. RDT-1B: A diffusion foundation model for bimanual manipulation. In *International Conference on Learning Representations*, 2025.

[Mildenhall *et al.*, 2020] Ben Mildenhall, Pratul P. Srinivasan, Matthew Tancik, Jonathan T. Barron, Ravi Ramamoorthi, and Ren Ng. Nerf: Representing scenes as neural radiance fields for view synthesis. In *Proceedings of the European Conference on Computer Vision (ECCV)*, 2020.

[Mu *et al.*, 2025] Yao Mu, Tianxing Chen, Zanxin Chen, Shijia Peng, Zhiqian Lan, Zeyu Gao, Zhixuan Liang, Qiaojun Yu, Yude Zou, Mingkun Xu, Lunkai Lin, Zhiqiang Xie, Mingyu Ding, and Ping Luo. Robotwin: Dual-arm robot benchmark with generative digital twins. In *Proceedings of the IEEE/CVF Conference on Computer Vision and Pattern Recognition (CVPR)*, pages 27649–27660, 2025.

[O’Neill *et al.*, 2024] Abby O’Neill, Abdul Rehman, Abhiram Maddukuri, Abhishek Gupta, Abhishek Padalkar, Abraham Lee, Acorn Pooley, Agrim Gupta, Ajay Mandekar, Ajinkya Jain, et al. Open X-embodiment: Robotic learning datasets and RT-X models. In *2024 IEEE International Conference on Robotics and Automation (ICRA)*, pages 6892–6903, 2024.

[Pang *et al.*, 2025] Jing-Cheng Pang, Nan Tang, kaiyuan Li, Yuting Tang, Xin-Qiang Cai, Zhen-Yu Zhang, Gang Niu, Sugiyama Masashi, and Yang Yu. Learning view-invariant world models for visual robotic manipulation. In *International Conference on Learning Representations (ICLR)*, 2025.

[Qian *et al.*, 2025] Shengyi Qian, Kaichun Mo, Valts Blukis, David F. Fouhey, Dieter Fox, and Ankit Goyal. 3D-MVP: 3D multiview pretraining for robotic manipulation. In *Proceedings of the IEEE/CVF Conference on Computer Vision and Pattern Recognition (CVPR)*, pages 22530–22539, 2025.

[Qu *et al.*, 2025] Delin Qu, Haoming Song, Qizhi Chen, Yuanqi Yao, Xinyi Ye, Jiayuan Gu, Zhigang Wang, Yan Ding, Bin Zhao, Dong Wang, and Xuelong Li. SpatialVLA: Exploring Spatial Representations for Visual-Language-Action Models. In *Proceedings of Robotics: Science and Systems*, Los Angeles, CA, USA, June 2025.

[Schönberger and Frahm, 2016] Johannes L. Schönberger and Jan-Michael Frahm. Structure-from-motion revisited. In *Proceedings of the IEEE Conference on Computer Vision and Pattern Recognition (CVPR)*, June 2016.

[Seo *et al.*, 2023] Younggyo Seo, Junsu Kim, Stephen James, Kimin Lee, Jinwoo Shin, and Pieter Abbeel. Multi-view masked world models for visual robotic manipulation. In *Proceedings of the 40th International Conference on Machine Learning*, volume 202 of *Proceedings of Machine Learning Research*, pages 30623–30640. PMLR, 2023.

[Sun *et al.*, 2025] Lin Sun, Bin Xie, Yingfei Liu, Hao Shi, Tiancai Wang, and Jiale Cao. Geovla: Empowering 3d representations in vision-language-action models. *arXiv preprint arXiv:2508.09071*, 2025.

[Wang *et al.*, 2025] Jianyuan Wang, Minghao Chen, Nikita Karaev, Andrea Vedaldi, Christian Rupprecht, and David Novotny. Vggt: Visual geometry grounded transformer. In *Proceedings of the IEEE/CVF Conference on Computer Vision and Pattern Recognition (CVPR)*, pages 20010–20020, June 2025.

[Yang *et al.*, 2025] Ruijia Yang, Geng Chen, Chuan Wen, and Yang Gao. Fp3: A 3d foundation policy for robotic manipulation. *arXiv preprint arXiv:2503.08950*, 2025.

[Yao *et al.*, 2018] Yao Yao, Zixin Luo, Shiwei Li, Tian Fang, and Long Quan. Mvsnet: Depth inference for unstructured multi-view stereo. In *Proceedings of the European Conference on Computer Vision (ECCV)*, 2018.

[Ze *et al.*, 2024] Yanjie Ze, Gu Zhang, Kangning Zhang, Chenyuan Hu, Muhan Wang, and Huazhe Xu. 3D Diffusion Policy: Generalizable Visuomotor Policy Learning via Simple 3D Representations. In *Proceedings of Robotics: Science and Systems*, Delft, Netherlands, July 2024.

[Zhao *et al.*, 2023] Tony Z. Zhao, Vikash Kumar, Sergey Levine, and Chelsea Finn. Learning Fine-Grained Bimanual Manipulation with Low-Cost Hardware. In *Proceedings of Robotics: Science and Systems*, Daegu, Republic of Korea, July 2023.

[Zitkovich *et al.*, 2023] Brianna Zitkovich, Tianhe Yu, Sichun Xu, Peng Xu, Ted Xiao, Fei Xia, Jialin Wu, Paul Wohlhart, Stefan Welker, Ayzaan Wahid, et al. RT-2: Vision-language-action models transfer web knowledge to robotic control. In *Proceedings of The 7th Conference on Robot Learning*, volume 229 of *Proceedings of Machine Learning Research*, pages 2165–2183. PMLR, 2023.

## A Implementation Details

**Overview.** Key hyperparameters and architectural settings are summarized in Tab. 5; in this Appendix we only describe implementation details that are not fully specified in the main text.

**Decoder upsampling head.** Following SEM, the decoder predicts  $H=64$  steps using a coarse-to-fine upsampling head: the base chunk length is  $H/c=8$  and is progressively upsampled to  $(16, 32, 64)$  with 1D convolutions (kernel size 3), using channel dimensions  $(256 \rightarrow 128 \rightarrow 64 \rightarrow 8)$ . At deployment, we run closed-loop control by executing  $H_{exec} = 32$  predicted actions per inference step.

## B Language-Guided Multi-View Readout

**Frozen CLIP features.** We use a frozen CLIP ViT-L/14 encoder. For each view  $v$ , we extract patch tokens  $\mathbf{X}^{(v)} \in \mathbb{R}^{N_p \times D_c}$  from the *attn-last* output (excluding the CLS token, following ClearCLIP), and extract text tokens  $\mathbf{T}_{\text{txt}} \in \mathbb{R}^{K_{\text{txt}} \times D_c}$  from the CLIP text encoder. We keep the first  $K_{\text{txt}}=64$  text tokens with a mask excluding SOT/EOT/PAD.

**Vision-grounded text tokens via Perceiver-style latent blocks.** For each view, we initialize latents with text tokens,  $\mathbf{Z}^{(v,0)} = \mathbf{T}_{\text{txt}}$ , and apply  $M=3$  latent blocks. Each latent block alternates (i) cross-attention where text latents query patch tokens and (ii) latent self-attention, with FFNs after each attention module. To stabilize stacking, we adopt ReZero-style gated residuals; concretely, for an operator  $F(\cdot)$  we use  $\mathbf{z} \leftarrow \mathbf{z} + \alpha F(\text{LN}(\mathbf{z}))$  with learnable gates  $\alpha$  initialized to zero. The final latents  $\mathbf{Z}^{(v)} \triangleq \mathbf{Z}^{(v,M)}$  serve as view-specific vision-grounded text tokens.

## C Depth Distillation Pipeline

**Training-only teacher depths.** We use a pretrained Camera Depth Model (CDM) offline to produce refined depths  $\tilde{\mathbf{D}}^{(v)}$  for each training frame. During both training and inference, the policy input remains the raw commodity depth  $\mathbf{D}^{(v)}$ ; CDM is never executed in the policy loop.

**Soft depth-bin targets.** For each pixel depth value  $\tilde{d}$ , we form a soft bin target by linear interpolation to its two nearest bin centers (Tab. 5,  $B=128$  linear bins in  $[d_{\min}, d_{\max}]$ ), yielding a sparse 2-hot distribution. We then average-pool per-pixel distributions to per-token targets aligned with the tokenization strides  $(8, 16, 32, 64)$ . A validity weight  $\omega_n^{(v)}$  is computed as the fraction of valid pixels in the pooled region (threshold 0.5) and is used to downweight unreliable regions, matching the loss in Eq. 16 of the main paper.

**Remark on depth-loss divergence.** The depth-loss divergence reported in the main paper is consistently observed across different random seeds with the same training protocol and hyperparameters. All curves are logged from independent training runs under different seeds.

## D Protocol: DR Configuration and Real-Robot Camera Rig

### D.1 DR Setting in RoboTwin 2.0

We use the domain-randomized configuration in Tab. 6, perturbing both scene appearance (background and lighting) and geometry (table height) per episode to stress-test generalization under occlusions, distractors, and illumination shifts.

### D.2 Real-Robot Camera Rig and Preprocessing

We use four Intel RealSense D435 RGB-D cameras with aligned depth-to-color streams, publishing  $424 \times 240$  RGB and depth at 30 FPS. Extrinsics are provided by external rig calibration.

**Remap-based resizing reduces effective FOV and overlap.** Although the raw streams are  $424 \times 240$ , our preprocessing applies a calibration-preserving *remap* to a fixed target resolution  $320 \times 256$  with a fixed destination intrinsic matrix (used consistently throughout training and evaluation). Compared with naive resizing, this remap effectively crops the usable source region, yielding a narrower effective field-of-view. In practice, this substantially reduces cross-view overlap, which makes real-robot multi-view correspondence and fusion more challenging.

## E Multi-view Ablation

Removing the front view reduces the average success from 47.1% to 35.0%, with the largest drops on BR-RGB, PBF, and PEC, where global context helps disambiguate targets under DR. Keeping only the head view further degrades performance (26.8%), particularly on wrist-critical fine manipulation (e.g., HM and SB3), highlighting the necessity of wrist observations for reliable bimanual coordination.

Table 5: Key hyperparameters for **PEAfowl**.

Item	Setting
Cameras	$V=4$ views: front, head, left_wrist, right_wrist
Input resolution	$320 \times 256$ (W×H) RGB and depth
History steps	$H_{\text{obs}}=1$
Prediction horizon	$H=64$
Temporal upsampling factor	$c = 8$
Token embed dim	$d=256$
RGB encoder	Swin-T: depths [2,2,6,2], heads [3,6,12,24], win=7 (Grounding-DINO init)
RGB neck	ChannelMapper $\rightarrow d=256$ , $L = 4$ feature levels
Depth encoder	ResNet-34 (1-ch), base_channels=4
Depth neck	ChannelMapper $\rightarrow d_{\text{dep}}=32$ , $L = 4$ feature levels
Depth bins	$B=128$ , depth range $[d_{\text{min}}, d_{\text{max}}] = [0.01, 1.2]$ m (linear bins)
Depth head	2-layer MLP + softmax over $B$ bins
Depth GT pooling	strides (8,16,32,64), valid_threshold=0.5
Pairwise RGB–D fusion	2-token MHA (4 heads, dim=32) + FFN (32 $\rightarrow$ 128 $\rightarrow$ 32)
Cross-view aggregation	top- $K=16$ , temperature $\tau=0.08$ , residual gate init $\gamma_0=0.5$
Action decoder blocks	6 blocks (SEM order)
Cross-attn (img/temp/text)	RoPE attention, 8 heads; max_pos: img=32, temp=32, text=512
Diffusion (train)	DDPM, 1000 steps, squaredcos_cap_v2, predict sample
Diffusion (test)	DPM-Solver multistep, 10 denoising steps
Optimizer	AdamW, lr $1.414 \times 10^{-4}$ , wd $5 \times 10^{-4}$
Backbone lr	$0.1 \times$ base lr for RGB backbone params
LR schedule	warmup 500 iters (start_factor=0.001), milestone at $0.9 \times \text{max\_step}$ , decay factor 0.1
Batch size / max step	$16 / 4 \times 10^5$ updates
Data aug.	joint-state uniform noise $\pm 0.02$ (grippers: 0)
CLIP readout	frozen CLIP ViT-L/14
Text tokens	first- $K_{\text{txt}}=64$ tokens (mask excludes SOT/EOT/PAD)
Latent blocks	$M=3$ Perceiver-style latent blocks, heads=16
Readouts	$R=64$ per view, pooling layers=2, pooling heads=8

Table 6: **RoboTwin 2.0 DR configuration**.

Factor	Setting
Random background	enabled
Cluttered table (distractors)	enabled
Clean background rate	0.02
Random lighting	enabled
Crazy random lighting rate	0.05
Random table height	$\pm 0.05$ m
Random head-camera distance	0

Table 7: **Per-task multi-view ablation under the DR setting**. Success rate (%). “w/o Front” removes the front view; “Head-only” removes the front and both wrist views. Task abbr. follow the main paper.

Task	PEAfowl	w/o Front	Head-only
OM	34	24	24
SB3	34	23	6
SW3	66	61	50
BR-RGB	47	20	12
BR-Size	14	7	6
HM	26	11	2
OL	68	69	55
PBF	65	47	45
PEC	70	53	41
<b>Avg.</b>	47.1	35.0	26.8